Simulation of Three-Dimensional Optical Waveguides by a Full-Vector Beam Propagation Method

W. P. Huang, *Member, IEEE,* and C. L. Xu

Abstract—**Simulations of optical guided waves in three-dimensional waveguide structures by a full vector beam propagation method are described. Two sets of coupled equations governing the propagation of the transverse electric and magnetic fields are derived systematically. Polarization dependence and coupling due to the vectorial nature of the electromagnetic fields are considered in the formulations. The governing equations are solved subsequently by finite-difference schemes. The vector BPM is first assessed for a step-index circular fiber by comparing the numerical results with the exact analytical solutions. The guided modes of a rib waveguide are then investigated in detail. Comparisons among the scalar, semi-vector and full-vector simulations of the rib waveguide are made. Finally, polarization rotation of a periodically loaded rib waveguide operated fully based on the vector nature of the electromagnetic waves is modeled and simulated.**

I. Introduction

THE beam propagation method (BPM) has been one of the most popular approaches used in the modeling and simulation of electromagnetic wave propagation in guided-wave optoelectronic and fiber-optic devices [1]–[5]. A decided shortcoming of the various conventional beam propagation methods is that they only solve the scalar wave equation [6]–[11]. The vector properties of the electromagnetic waves have been ignored. Admittedly, the variations of the refractive index over the transverse dimensions are small and/or slow in most of practical optical waveguide structures. Consequently, the polarization dependence and coupling are weak and may be neglected for applications where the polarization is of no interest. However, the vector properties may become important and even essential if the polarization is of concern. For instance, large index variations do occur in some optical waveguide structures made of semiconductor materials. Even in the case of small index variations, the polarization behavior will become significant due to the long propagation distance with respect to the wavelength. Therefore, it is necessary to model and simulate the vectorial electromagnetic wave propagation in the optical guided-wave devices.

Manuscript received February 2, 1992; revised March 2, 1993. This work was supported in part by the Natural Science and Engineering Research Council and in part by the Canadian Institute for Telecommunications Research under the NCE program of the Government of Canada.

The authors are with the Department of Electrical and Computer Engineering, University of Waterloo, Waterloo, Ont., Canada N2L 3G1.

IEEE Log Number 9211551.

The vectorial guided waves in the form of the guided modes in a canonical, especially uniform (or z-invariant) optical waveguide have been modeled and analyzed by the effective index method [12], the variational and perturbation methods [13], the spectral index method [14], the finite-element method [15], and the finite-difference method [16]. Strictly speaking, all the above methods are semi-vector, i.e., only the polarization dependence of the vectorial modes is considered, except for the finite-element method in [15] where the full vector nature of the modes (i.e., hybrid modes) was considered. A theoretically more challenging and practically more urgent problem is to analyze and simulate the vectorial wave propagation through a non-canonical, i.e., nonuniform structure. The vector coupled-mode theory (CMT) of various forms [12], [17]–[21] can be applied to the analysis and simulation of vectorial waves as demonstrated for many two-dimensional waveguide structures. For the three-dimensional structures, however, the full vector CMT approach becomes less applicable due to the lack of simple analytical description of the vector modes. A scalar coupled-mode theory with vector correction has been advanced lately [22] and may be applied to some three-dimensional structures where the scalar modes can be obtained analytically or semi-analytically. Although this quasi-vectorial CMT has achieved certain level of success in modeling and analysis of the vectorial wave propagation in some devices [23], [24], its range of application and scope of validity may still be limited. In particular, it is usually difficult for the CMT to account for the radiation phenomenon, which is important for many practical guided-wave structures.

Considerable effort of the recent research is to extend the present BPM schemes to modeling and simulation of the vectorial wave propagation [25]–[27]. A vector BPM based on the finite-difference schemes (FD-VBPM) was developed and reported briefly [28], [29]. The analysis and assessment of the finite-difference vector beam propagation method (FD-VBPM) as it applies to two-dimensional structure has also been carried out [30] and the applications of the method to the two-dimensional coupler devices have been demonstrated [31]. In this article, a systematic development of the full vector beam propagation method is presented. The one-way propagation of the vectorial electromagnetic fields are governed by two sets of coupled equations for the transverse electric and magnetic fields, respectively. By solving these two sets of

coupled equations independently using finite-difference schemes, the propagation of vectorial guided-waves can be simulated explicitly as an initial value problem. The article is organized as follows: Section II establishes the mathematical formulations for the full vector BPM. The governing equations for the transverse electric and magnetic fields are derived and discussed. The finite-difference schemes used to solve the governing equations are described in Section III and the implementation of the solution schemes are discussed in Section IV. The FD-VBPM is validated in the case of a step-index fiber in Section V. The convergence, the numerical dispersion and dissipation of the FD-VBPM are examined. The applications of the method to some typical optical guided-wave structures are presented in Section VI. The simulations of the guided modes of an optical rib waveguide and the polarization rotation of a periodically loaded rib waveguide are described.

II. Formulations

In the frequency domain, the propagation of electromagnetic waves through a nonhomogeneous medium is governed by Maxwell's equations

$$\nabla \times \mathbf{E} = -j\omega\mu_0 \mathbf{H} \tag{1a}$$

$$\nabla \times \mathbf{H} = j\omega\epsilon_0 n^2 \mathbf{E} \tag{1b}$$

and

$$\nabla \cdot (n^2 \mathbf{E}) = 0 \tag{2a}$$

$$\nabla \cdot (\mathbf{H}) = 0 \tag{2b}$$

where $n = n(x, y, z)$ is the refractive index of the medium which is assumed to be isotropic. The material dispersion and absorption or gain can be described by the real and the imaginary parts of $n(x, y, z)$ as functions of frequency. A time dependence of $e^{j\omega t}$ has been assumed and factored out. One may solve the two curl equations (1a) and (1b) simultaneously in order to model and simulate the electromagnetic wave propagation in a medium characterized by n. As an alternative, a system of coupled vector wave equations for either the transverse electric or magnetic fields can be derived. The two sets of equations are decoupled and can be solved independently.

A. Full Vector Formulations

E-Formulation: The vector wave equation for the electric or magnetic fields

$$\nabla \times \nabla \times \mathbf{E} - n^2 k^2 \mathbf{E} = 0 \tag{3}$$

where $k = \omega\sqrt{\epsilon_0\mu_0}$ is the wave number in free space. By using the identity

$$\nabla \times \nabla \times = \nabla(\nabla \cdot) - \nabla^2 \tag{4}$$

the transverse components of (3) reduce to

$$\nabla^2 \mathbf{E}_t + n^2 k^2 \mathbf{E}_t = \nabla_t \left(\nabla_t \cdot \mathbf{E}_t + \frac{\partial E_z}{\partial z} \right). \tag{5}$$

Furthermore, (2a) yields

$$\nabla_t \cdot (n^2 \mathbf{E}_t) + \frac{\partial n^2}{\partial z} E_z + n^2 \frac{\partial E_z}{\partial z} = 0. \tag{6}$$

If the refractive index varies slowly along z, then $(\partial n^2/\partial z)E_z$ may be neglected. Equation (6) is approximated by

$$\frac{\partial E_z}{\partial z} \approx -\frac{1}{n^2} \nabla_t \cdot (n^2 \mathbf{E}_t) \tag{7}$$

which is exact for uniform (or z-invariant) structures. Substitute (7) into (5)

$$\nabla^2 \mathbf{E}_t + n^2 k^2 \mathbf{E}_t = -\nabla_t (\nabla_t \ln n^2 \cdot \mathbf{E}_t) \tag{8}$$

or written in terms of the x and y components

$$\nabla^2 E_x + n^2 k^2 E_x = -\frac{\partial}{\partial x}\left(\frac{\partial \ln n^2}{\partial x} E_x \right) - \frac{\partial}{\partial x}\left(\frac{\partial \ln n^2}{\partial y} E_y \right) \tag{9a}$$

$$\nabla^2 E_y + n^2 k^2 E_y = -\frac{\partial}{\partial y}\left(\frac{\partial \ln n^2}{\partial x} E_x \right) - \frac{\partial}{\partial y}\left(\frac{\partial \ln n^2}{\partial y} E_y \right). \tag{9b}$$

Assume that

$$\mathbf{E}_t = \hat{\mathbf{E}}_t e^{-jn_0 kz} \tag{10}$$

where n_0 is a reference refractive index. Substitute (10) into (8) or (9) and make use of the slowly varying envelope approximation, i.e.,

$$\left| \frac{\partial^2 \hat{\mathbf{E}}_t}{\partial z^2} \right| \ll 2n_0 k \left| \frac{\partial \hat{\mathbf{E}}_t}{\partial z} \right|. \tag{11}$$

We obtain the paraxial vector wave equations

$$j\frac{\partial \hat{E}_x}{\partial z} = A_{xx}\hat{E}_x + A_{xy}\hat{E}_y \tag{12a}$$

$$j\frac{\partial \hat{E}_y}{\partial z} = A_{yy}\hat{E}_y + A_{yx}\hat{E}_x \tag{12b}$$

where the differential operators are defined by

$$A_{xx}\hat{E}_x = \frac{1}{2n_0 k}\left\{ \frac{\partial}{\partial x}\left[\frac{1}{n^2}\frac{\partial}{\partial x}(n^2 \hat{E}_x) \right] + \frac{\partial^2}{\partial y^2}\hat{E}_x + (n^2 - n_0^2)k^2 \hat{E}_x \right\} \tag{13a}$$

$$A_{yy}\hat{E}_y = \frac{1}{2n_0 k}\left\{ \frac{\partial^2}{\partial x^2}\hat{E}_y + \frac{\partial}{\partial y}\left[\frac{1}{n^2}\frac{\partial}{\partial y}(n^2 \hat{E}_y) \right] + (n^2 - n_0^2)k^2 \hat{E}_y \right\} \tag{13b}$$

$$A_{xy}\hat{E}_y = \frac{1}{2n_0 k}\left\{ \frac{\partial}{\partial x}\left[\frac{1}{n^2}\frac{\partial}{\partial y}(n^2 \hat{E}_y) \right] - \frac{\partial^2}{\partial x \partial y}\hat{E}_y \right\} \tag{13c}$$

$$A_{yx}\hat{E}_x = \frac{1}{2n_0k}\left\{\frac{\partial}{\partial y}\left[\frac{1}{n^2}\frac{\partial}{\partial x}(n^2\hat{E}_x)\right] - \frac{\partial^2}{\partial y\,\partial x}\hat{E}_x\right\}. \quad (13d)$$

From (12), we see that the vector nature of the electromagnetic waves dictates that the transverse electric field components are polarization-dependent and coupled with each other. The operators A_{ij} $(i, j = x, y)$ show that the vectorial properties become important when the variation of the refractive index over the transverse cross section is fast and/or the difference at the index discontinuities is large. The boundary conditions for the transverse electric fields are also contained in the operators. The discontinuities of E_x and E_y across the index interfaces along x and y directions are responsible for the polarization dependence (i.e., $A_{xx} \neq A_{yy}$) and coupling (i.e., A_{xy} and $A_{yx} \neq 0$).

H-Formulation: Similarly to the vector wave equations for the electric field, the equations for the magnetic fields read

$$\nabla \times \nabla \times \mathbf{H} - n^2k^2\mathbf{H} - \frac{1}{n^2}\nabla n^2 \times (\nabla \times \mathbf{H}) = 0. \quad (14)$$

The transverse components of (14) can be approximated by

$$\nabla^2 H_x + n^2k^2H_x - \frac{1}{n^2}\frac{\partial n^2}{\partial y}\left(\frac{\partial H_x}{\partial y} - \frac{\partial H_y}{\partial x}\right) = 0 \quad (15a)$$

$$\nabla^2 H_y + n^2k^2H_y - \frac{1}{n^2}\frac{\partial n^2}{\partial x}\left(\frac{\partial H_y}{\partial x} - \frac{\partial H_x}{\partial y}\right) = 0. \quad (15b)$$

By letting

$$\mathbf{H}_t = \hat{\mathbf{H}}_t e^{-jkn_0z} \quad (16)$$

and assuming the slowly varying envelope approximation, i.e.,

$$\left|2kn_0\frac{\partial \hat{\mathbf{H}}_t}{\partial z}\right| \gg \left|\frac{\partial^2 \hat{\mathbf{H}}_t}{\partial z^2}\right| \quad (17)$$

(15) reduces to

$$j\frac{\partial \hat{H}_x}{\partial z} = B_{xx}\hat{H}_x + B_{xy}\hat{H}_y \quad (18a)$$

$$j\frac{\partial \hat{H}_y}{\partial z} = B_{yy}\hat{H}_y + B_{yx}\hat{H}_x \quad (18b)$$

where the operators in (18) are defined as

$$B_{xx}\hat{H}_x = \frac{1}{2kn_0}\left\{\frac{\partial^2 \hat{H}_x}{\partial x^2} + n^2\left[\frac{\partial}{\partial y}\left(\frac{1}{n^2}\frac{\partial \hat{H}_x}{\partial y}\right)\right] + (n^2 - n_0^2)k^2\hat{H}_x\right\} \quad (19a)$$

$$B_{yy}\hat{H}_y = \frac{1}{2kn_0}\left\{\frac{\partial^2 \hat{H}_y}{\partial y^2} + n^2\left[\frac{\partial}{\partial x}\left(\frac{1}{n^2}\frac{\partial \hat{H}_y}{\partial x}\right)\right] + (n^2 - n_0^2)k^2\hat{H}_y\right\} \quad (19b)$$

$$B_{xy}\hat{H}_y = \frac{1}{2kn_0}\left\{\frac{\partial^2 \hat{H}_y}{\partial y\,\partial x} - n^2\left[\frac{\partial}{\partial y}\left(\frac{1}{n^2}\frac{\partial \hat{H}_y}{\partial x}\right)\right]\right\} \quad (19c)$$

$$B_{yx}\hat{H}_x = \frac{1}{2kn_0}\left\{\frac{\partial^2 \hat{H}_x}{\partial x\,\partial y} - n^2\left[\frac{\partial}{\partial x}\left(\frac{1}{n^2}\frac{\partial \hat{H}_x}{\partial y}\right)\right]\right\} \quad (19d)$$

and the reference index n_0 is to be determined so that the slowly varying envelope approximations in (17) are satisfied. The boundary conditions for the transverse magnetic fields are contained in the operators defined by (19). For instance, the discontinuities of $\partial\hat{H}_x/\partial y$ and $\partial\hat{H}_y/\partial x$ across the index interfaces along y and x directions are responsible for the polarization dependence (i.e., $B_{xx} \neq B_{yy}$) and coupling (i.e., B_{xy} and $B_{yx} \neq 0$).

Hence, (12) and (18) govern the propagation of the vector waves in the medium under the condition that the refractive index varies slowly along the direction of wave propagation. The equations for the transverse E and H fields are decoupled so that they can be solved independently. For a two-dimensional structure, there is no coupling between the two polarizations, i.e, $A_{xy} = A_{yx} = 0$ and $B_{xy} = B_{yx} = 0$. The vector waves may be decomposed into the TE (y-polarized transverse E-field and x-polarized transverse H-field) and TM (x-polarized transverse E-field and y-polarized H-field) waves which can be treated separately by solving (12a), (12b) and (18a), (18b) independently.

Once the transverse electric and magnetic fields are found, the guided power along z can be calculated by the integral

$$P(z) = \frac{1}{4}\int (\hat{\mathbf{E}}_t^* \times \hat{\mathbf{H}}_t + \hat{\mathbf{E}}_t \times \hat{\mathbf{H}}_t^*) \cdot \hat{z}\, da. \quad (20)$$

B. Semi-Vector Formulations

For three-dimensional structures, the polarization couplings usually exist so that the propagating waves are, strictly speaking, hybrid. However, the couplings between the two polarizations are usually weak and may not have appreciable effect unless the two polarizations are synchronized. Therefore, we may still neglect the coupling terms and treat the two polarizations independently by using a semi-vector beam propagation method to solve (12) and (18). The governing equations for the semi-vector BPM are

$$j\frac{\partial \hat{E}_x}{\partial z} = A_{xx}\hat{E}_x \quad (21a)$$

$$j\frac{\partial \hat{E}_y}{\partial z} = A_{yy}\hat{E}_y \quad (12b)$$

for the transverse electric fields and

$$j\frac{\partial \hat{H}_x}{\partial x} = B_{xx}\hat{H}_x \quad (22a)$$

$$j\frac{\partial \hat{H}_y}{\partial z} = B_{yy}\hat{H}_y \quad (22b)$$

for the transverse magnetic fields. Under the semi-vector approximations, the polarization dependences of the EM waves are taken into account.

C. Scalar Formulation

If the structures are weakly guiding and/or the polarization dependence is not at the issue, then the polarization dependence of the propagating waves may be neglected. Under the scalar approximation, (21) and (22) are replaced by a single wave equation

$$j\frac{\partial \Psi}{\partial z} = H\Psi \tag{23}$$

where Ψ stands for the transverse electric or magnetic fields and both Ψ and its first-order derivatives are assumed to be continuous. The operator is defined as

$$H = \frac{1}{2n_0 k}\left\{\frac{\partial^2}{\partial x^2} + \frac{\partial^2}{\partial y^2} + (n^2 - n_0^2)k^2\right\}. \tag{24}$$

Equation (23) is the governing equation for the conventional scalar beam propagation method.

III. Finite-Difference Schemes

Equations (12) and (18) and their reduced semi-vector forms (20) and (21) and scalar form (23) can all be solved by using a finite-difference method. In the finite-difference solutions, the continuous space is replaced by a discrete lattice structure defined in the computation region. The fields at the lattice point of $x = m\Delta x$, $y = n\Delta y$, and $x = l\Delta z$ are represented by their discrete versions. The operators in the E- and H-formulations are also approximated by the finite-difference. The discrete form of the differential operators in the governing equations (13) and (19) may be found in a straightforward way. At the index discontinuities, although the normal electric fields are not continuous, the displacement vectors $n^2\hat{E}_x$ are continuous across the index interfaces along the x- and y-axis, respectively. Therefore the central difference scheme can be applied directly. No special treatments as done in [16] are needed. The expressions for the operators are found to be as follows.

E-Formulation

$$A_{xx}\hat{E}_x = \frac{1}{2n_0 k}\left\{\frac{T^E_{m+1,n}\hat{E}_x(m+1,n) - [2 - R^E_{m+1,n} - R^E_{m-1,n}]\hat{E}_x(m,n) + T^E_{m-1,n}\hat{E}_x(m-1,n)}{(\Delta x)^2}\right.$$
$$\left. + \frac{\hat{E}_x(m,n+1) - 2\hat{E}_x(m,n) + \hat{E}_x(m,n-1)}{(\Delta y)^2} + [n^2(m,n,l) - n_0^2]k^2\hat{E}_x(m,n)\right\} \tag{25}$$

where

$$T^E_{m\pm1,n} = \frac{2n^2(m \pm 1, n, l)}{n^2(m \pm 1, n, l) + n^2(m, n, l)} \tag{26a}$$

$$R^E_{m\pm1,n} = T^E_{m\pm1,n} - 1 \tag{26b}$$

are the transmission and the reflection coefficients across the index interfaces between $m\Delta x$ and $(m+1)\Delta x$.

$$A_{yy}\hat{E}_y = \frac{1}{2n_0 k}\left\{\frac{T^E_{m,n+1}\hat{E}_y(m,n+1) + [2 - R^E_{m,n+1} - R^E_{m,n+1}]\hat{E}_y(m,n) + T_{m,n-1}\hat{E}_y(m,n-1)}{(\Delta y)^2}\right.$$
$$\left. + \frac{\hat{E}_y(m+1,n) - 2\hat{E}_y(m,n) + \hat{E}_y(m-1,n)}{(\Delta x)^2} - [n^2(m,n,l) - n_0^2)]k^2\hat{E}_y(m,n)\right\} \tag{27}$$

where

$$T^E_{m,n\pm1} = \frac{2n^2(m, n \pm 1, n, l)}{n^2(m, n \pm 1, l) + n^2(m, n, l)} \tag{28a}$$

$$R^E_{m,n\pm1} = T^E_{m,n\pm1} - 1 \tag{28b}$$

are the transmission and the reflection coefficients across the index interfaces between $n\Delta y$ and $(n+1)\Delta y$. Similarly, A_{xy} and A_{yx} are expressed by

$$A_{xy}\hat{E}_y = \frac{1}{8n_0 k\Delta x\Delta y}\left\{\left[\frac{n^2(m+1,n+1,l)}{n^2(m+1,n,l)} - 1\right]\right.$$
$$\cdot \hat{E}_y(m+1,n+1)$$
$$- \left[\frac{n^2(m+1,n-1,l)}{n^2(m+1,n,l)} - 1\right]$$
$$\cdot \hat{E}_y(m+1,n-1)$$
$$- \left[\frac{n^2(m-1,n+1,l)}{n^2(m-1,n,l)} - 1\right]$$
$$\cdot \hat{E}_y(m-1,n+1)$$
$$+ \left[\frac{n^2(m-1,n-1,l)}{n^2(m-1,n,l)} - 1\right]$$
$$\left. \cdot \hat{E}_y(m-1,n-1)\right\} \tag{29a}$$

$$A_{yx}\hat{E}_x = \frac{1}{8n_0k\Delta y\Delta x}\left\{\left[\frac{n^2(m+1,n+1,l)}{n^2(m,n+1,l)}-1\right]\cdot\hat{E}_x(m+1,n+1)-\left[\frac{n^2(m-1,n+1,l)}{n^2(m,n-1,l)}-1\right]\cdot\hat{E}_x(m-1,n+1)-\left[\frac{n^2(m+1,n-1,l)}{n^2(m,n+1,l)}-1\right]\cdot\hat{E}_x(m+1,n-1)+\left[\frac{n^2(m-1,n-1,l)}{n^2(m,n-1,l)}-1\right]\cdot\hat{E}_x(m-1,n-1)\right\} \quad (29b)$$

H-Formulation

$$B_{xx}\hat{H}_x = \frac{1}{2n_0k}\left\{\frac{\hat{H}_x(m+1,n)-2\hat{H}_x(m,n)+H_x(m-1,n)}{(\Delta x)^2}+\frac{T^H_{m,n+1}\hat{H}_x(m,n+1)-[T^H_{m,n+1}+T^H_{m,n-1}]\hat{H}_x(m,n)+T^T_{m,n-1}\hat{H}_x(m,n-1)}{(\Delta y)^2}-[n^2(m,n,l)-n_0^2)]k^2\hat{H}_x(m,n)\right\} \quad (30a)$$

$$B_{yy}\hat{H}_y = \frac{1}{2n_0k}\left\{\frac{\hat{H}_y(m,n+1)-2\hat{H}_y(m,n)+\hat{H}_y(m,n-1)}{(\Delta y)^2}+\frac{T^H_{m+1,n}\hat{H}_y(m+1,n)-[T^H_{m+1,n}+T^H_{m-1,n}]\hat{H}_y(m,n)+T^H_{m-1,n}\hat{H}_y(m-1,n)}{(\Delta x)^2}-[n^2(m,n,l)-n_0^2)]k^2\hat{H}_y(m,n)\right\} \quad (30b)$$

where

$$T^H_{m,n\pm1} = \frac{2n^2(m,n,l)}{n^2(m,n\pm1,l)+n^2(m,n,l)} \quad (31a)$$

and

$$T^H_{m\pm1,n} = \frac{2n^2(m,n,l)}{n^2(m\pm1,n,l)+n^2(m,n,l)}. \quad (31b)$$

Similarly, B_{xy} and B_{yx} are expressed by

$$B_{xy}\hat{H}_y = \frac{1}{8n_0k\Delta x\Delta y}\left\{\left[1-\frac{n^2(m,n,l)}{n^2(m,n+1,l)}\right]\cdot\hat{H}_y(m+1,n+1)-\left[1-\frac{n^2(m,n,l)}{n^2(m,n-1,l)}\right]\hat{H}_y(m+1,n-1)-\left[1-\frac{n^2(m,n,l)}{n^2(m,n+1,l)}\right]\hat{H}_y(m-1,n+1)+\left[1-\frac{n^2(m,n,l)}{n^2(m,n-1,l)}\right]\hat{H}_y(m-1,n-1)\right\} \quad (32a)$$

$$B_{yx}\hat{H}_x = \frac{1}{8n_0k\Delta y\Delta x}\left\{\left[1-\frac{n^2(m,n,l)}{n^2(m+1,n,l)}\right]\cdot\hat{H}_x(m+1,n+1)-\left[1-\frac{n^2(m,n,l)}{n^2(m-1,n,l)}\right]\hat{H}_x(m-1,n+1)-\left[1-\frac{n^2(m,n,l)}{n^2(m+1,n,l)}\right]\hat{H}_x(m+1,n-1)+\left[1-\frac{n^2(m,n,l)}{n^2(m-1,n,l)}\right]\hat{H}_x(m-1,n-1)\right\}. \quad (32b)$$

A set of finite-difference equations can be derived

$$[1+j\Delta z\alpha A_{xx}]\hat{E}_x^{l+1} = [1-j\Delta z(1-\alpha)A_{xx}]\hat{E}_x^l - j\Delta z A_{xy}\hat{E}_y^l \quad (33a)$$

$$[1+j\Delta z\alpha A_{yy}]\hat{E}_y^{l+1} = [1-j\Delta z(1-\alpha)A_{yy}]\hat{E}_y^l - j\Delta z A_{yx}\hat{E}_x^l \quad (33b)$$

for the transverse electric fields and

$$[1+j\Delta z\alpha B_{xx}]\hat{H}_x^{l+1} = [1-j\Delta z(1-\alpha)B_{xx}]\hat{H}_x^l - j\Delta z B_{xy}\hat{H}_y^l \quad (34a)$$

$$[1+j\Delta z\alpha B_{yy}]\hat{H}_y^{l+1} = [1+j\Delta z(1+\alpha)B_{yy}]\hat{H}_y^l - j\Delta z B_{yx}\hat{H}_x^l \quad (34b)$$

for the transverse magnetic fields. The parameter α is introduced to control the schemes used to solve the finite-difference equations.

IV. Implementation

An iterative procedure can be carried out to solve the coupled equations (33) and (34) for the transverse electric and magnetic fields, respectively. At each iteration step, a matrix equation is solved by employing the ORTHOMIN algorithm [32]. The operation count for the

matrix solvers is proportional to the order of the matrix N in comparison with the Fast Fourier Transform (FFT) in the conventional BPM whose operation count is proportional to $N \log N$. In the vector BPM, however, two pairs of coupled equations instead of one single equation as in the scalar BPM need to be solved. Therefore, approximately four times of computation is required if one is interested in both the electric and the magnetic fields or the power. A much more efficient (with reduction of nearly half of the computation) but may be less accurate approach is to first calculate only one set of transverse field, for instance, the H-field, and then derive the other set, i.e., the E-field, from the known transverse fields by numerical differentiation.

At the edges of the computation window, a numerical boundary condition which is transparent to the traveling waves towards the edges is implemented [33]. For instance, near the boundary at the right end of the computation window along the x-axis (i.e., $x = M\Delta x$), the field should satisfy

$$\frac{\partial \Psi}{\partial x} = -jk_x \Psi \tag{35}$$

or in the finite-difference form

$$\Psi^{l+1}(M, n) = \Psi_x^{l+1}(M - 1, n) e^{-jk_x \Delta x} \tag{36}$$

where the transverse complex wave vector is computed from the previous step by calculating the ratio $\Psi^l(M - 1, n)/\Psi^l(M - 2, n)$. The transparent boundary conditions are superior to the conventional absorbing boundary conditions because they are more efficient and accurate. In addition, the implementation of the transparent boundary conditions is relatively independent of the waveguide structures simulated and therefore is more robust.

The reference index n_0 should be chosen so that the slowly varying envelope approximations in (5) are valid. If the difference of the refractive index over the transverse cross section is small, one may chose n_0 to be the refractive index of the cladding. Otherwise, one has to choose n_0 with caution so that the variations of $\hat{\mathbf{E}}_t$ and $\hat{\mathbf{H}}_t$ along the longitudinal direction z are minimized. To satisfy this requirement, the optimum refractive index should be the average of the effective indices of all the guided-modes involved in the propagation process. For single-mode waveguides, the reference index n_0 can be chosen as the effective index of the local guided-mode

$$n_0 = \frac{\beta}{k} \tag{37}$$

where β is the propagation constant of the fundamental local mode of the canonical waveguide defined at z. For dual-mode waveguides such as directional couplers, the reference index can be chosen as

$$n_0 = \frac{\beta_S + \beta_A}{2k} \tag{38}$$

where β_S and β_A are the propagation constants of the symmetric and antisymmetric local guided modes. When no guided modes can be clearly identified or the propagation constants of the guided modes are not known, the reference index may be approximated by a weighted average of the refractive index profile over the entire cross section. A possible approach to overcome the problem for the choice of the reference index may be wide-angle or even higher-order schemes applied in the scalar BPM [34].

V. Validations

The analysis and assessment of the FD-VBPM for the two-dimensional structures have been presented in [30]. The results obtained can be equally applied to the semi-vectorial FD-VBPM for the three-dimensional structures. A general analysis of the finite-difference schemes used in the FD-VBPM regarding the numerical stability, dissipation and dispersion, however, appears to be difficult and has not yet been carried out. Instead, we investigated some important aspects of the FD-VBPM by examining a step-index circular fiber to which the exact analytical solutions are known and can be used for comparison. The refractive indices of the core and cladding are $n_1 = 1.469$ and $n_2 = 1.460$, respectively. The radius is $a = 3$ μm. The wavelength is $\lambda = 1.55$ μm.

By propagating an arbitrary field along imaginary distance using FD-VBPM, one can efficiently calculate the propagation constant and the corresponding field pattern of the fundamental model [35]. Figs. 1 and 2 show the patterns of the transverse electric and magnetic fields for the fundamental HE_{11} mode generated by the FD-VBPM, respectively. The computation window is $W_x = W_y = 12$ μm and there are 101×101 grid points in the computation window. The corresponding field patterns produced by the exact solutions with the same resolution (i.e., the same number of grid points in the computation window) are also displayed. The field patterns predicted by the FD-VBPM are in excellent agreement with the exact solutions except that some numerical noises appear near the core-cladding interface for the minor electric field component E_y.

Figs. 3(a) and (b) show the percentage error in the normalized propagation constant $b = (\beta^2 - n_2^2 k^2)/(n_1^2 - n_2^2)k^2$ and the attenuation due to the numerical dispersion of the HE_{11} mode as functions of the longitudinal step size Δz. The scheme parameter is chosen to be $\alpha = 1.0$ (solid) and $\alpha = 0.5$ (dash), respectively. The transverse step sizes are $\Delta x = \Delta y = 0.12$ μm. It is noted that the percentage error is almost independent of the longitudinal step size Δz and the scheme parameter α. The attenuation which is measured by the total insertion loss in decibels for the length of $L = 20$ μm decreases slightly with the increase of Δz. This behavior is somewhat peculiar and has not yet been explained. In addition, the scheme parameter α also affects the attenuation and the smaller value of α seems to lead to larger numerical dissipation. Figs. 4(a) and (b) show the percentage error in the propagation constant and the attenuation due to the numerical dissipation of the HE_{11} mode as functions of the transverse step sizes. Δz

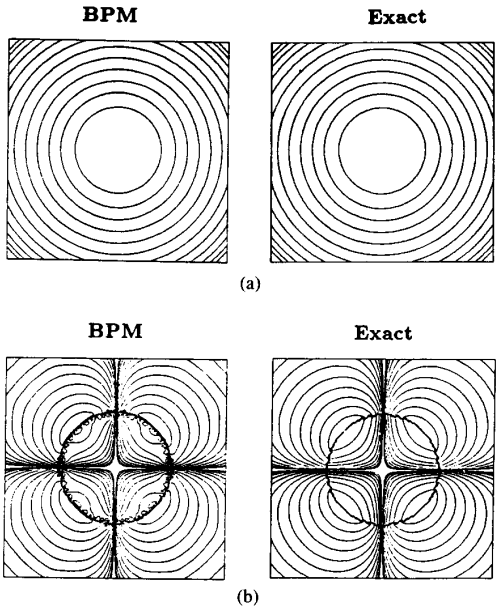

Fig. 1. Field patterns of the transverse electric fields of the HE_{11} mode in a step-index circular fiber. Comparisons are made between the BPM simulation and the exact solutions. (a) E_x; (b) E_y.

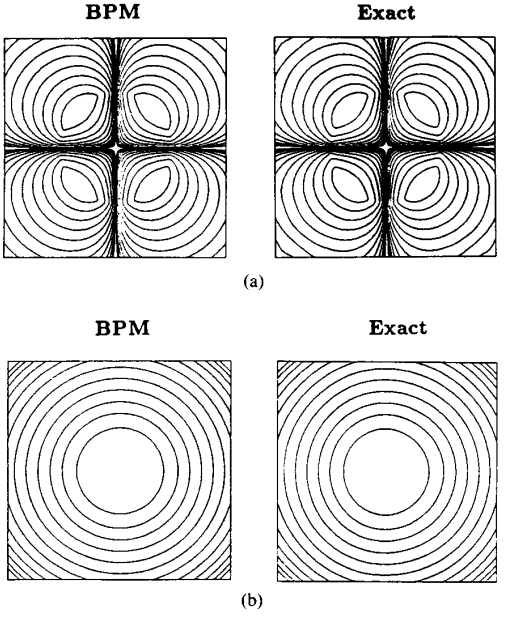

Fig. 2. Field patterns of the transverse magnetic fields of the HE_{11} mode in a step-index circular fiber. Comparisons are made between the BPM simulation and the exact solutions. (a) H_x; (b) H_y.

$= 0.5$ μm is assumed. The error in the normalized propagation constant b and the numerical attenuation depends critically on the transverse step sizes. The BPM solutions appear to converge to the exact solutions as the transverse step sizes go to zero. Also, it is seen that the scheme parameter α affects only the accuracy in the amplitude of

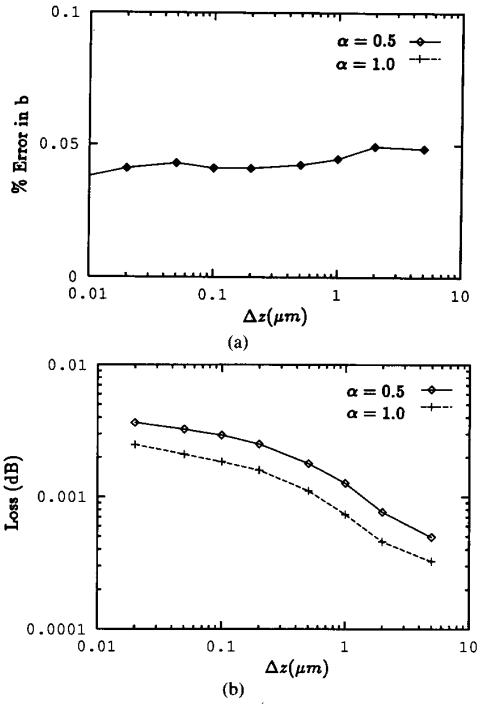

Fig. 3. The accuracy of HE_{11} mode of a step-index circular fiber predicted by the BPM as function of the longitudinal step size Δz. The window sizes are $W_x = W_y = 12$ μm and the number of grid points are 101×101. (a) The percentage error in the normalized propagation constant. (b) The power attenuation for a total length of 20 μm.

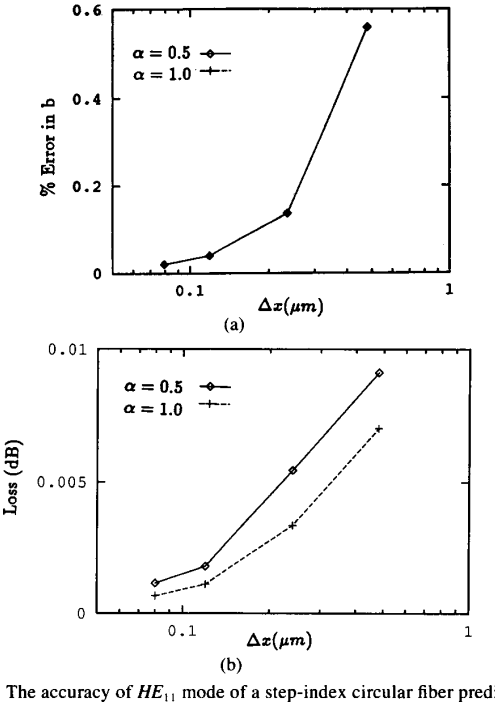

Fig. 4. The accuracy of HE_{11} mode of a step-index circular fiber predicted by the BPM as function of the transverse step size $\Delta x = \Delta y$. The window sizes are $W_x = W_y = 12$ μm and the longitudinal step size is $\Delta z = 0.1$ μm. (a) The percentage error in the normalized propagation constant. (b) The power attenuation for a total length of 20 μm.

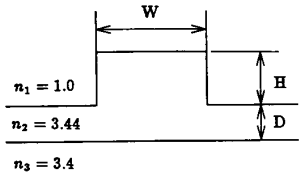

Fig. 5. The geometry of the optical rib waveguide simulated.

the waves (i.e., the attenuation) but not the phase (i.e., the percentage error in the propagation constant). In all the simulations, the numerical schemes are found to be stable.

VI. Applications

A. Guided-Modes in Optical Rib Waveguide

A typical rib waveguide structure is depicted in Fig. 5. The refractive indices of the guiding, substrate and the cover layers are $n_3 = 3.44$, $n_2 = 3.4$,and $n_1 = 1.0$. The wavelength is assumed to be $\lambda = 1.15$ μm. The transverse electric field patterns of the quasi-TE and quasi-TM modes are calculated by the imaginary-distance propagation method and shown in Figs. 6 and 7, respectively. The dimensions of the waveguides are $D = H = 0.5$ μm and $W = 3.0$ μm. The discontinuities of the normal electric fields across the index interfaces and the hybrid nature of the modes are clearly demonstrated in both cases. We also calculated the normalized propagation constants of the two modes for different D and the results are shown in Table I. We also listed the normalized propagation constants predicted by the semi-vector and the scalar BPM's. It is seen that the difference between the semi- and the full-vector BPMs is small. In practice, unless the polarization dependence of the propagating wave is of interest, the hybrid nature (or the polarization coupling) can be neglected and the semi-vector BPM should be sufficient. The results reported in [16] by using the semi-vectorial finite-difference method are also included in the table for the sake of comparison. The differences between the BPM and the FD are very small.

B. Polarization Rotation in Periodically Loaded Rib Waveguide

The cross-sectional and the top views of the periodically loaded rib waveguide is shown in Fig. 8. A similar structure has been used by Shani and coworkers [36] experimentally to achieve polarization rotation. A coupled-mode analysis of this device has been proposed [24] and indicates that the polarization rotation is purely due to the vectorial properties of the guided modes in the asymmetrically loaded rib waveguide. A simulation by the FD-VBPM is carried out in the this article. In comparison with the intuitive coupled-mode analysis, the VBPM simulation is expected to be more accurate. In particular, the scattering loss at each junction can be predicted by the VBPM.

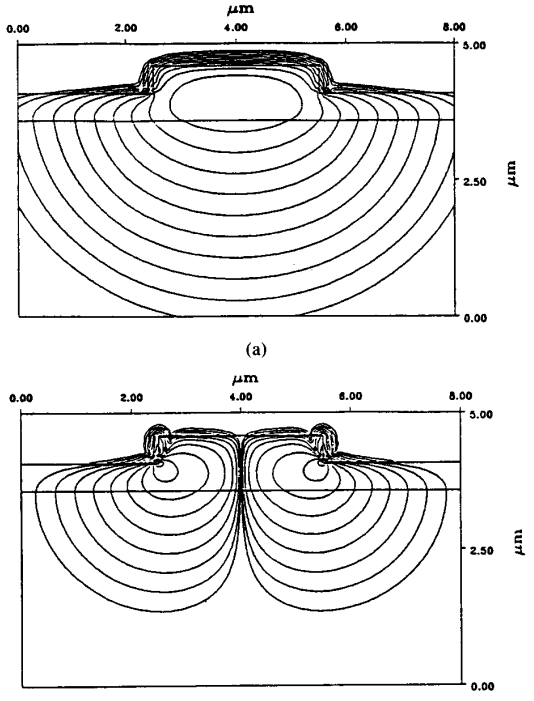

Fig. 6. The patterns of the transverse electric field for the quasi-TE mode of the rib waveguide. The waveguide parameters are $W = 3.0$ μm and $D = H = 0.5$ μm. (a) E_x; (b) E_y.

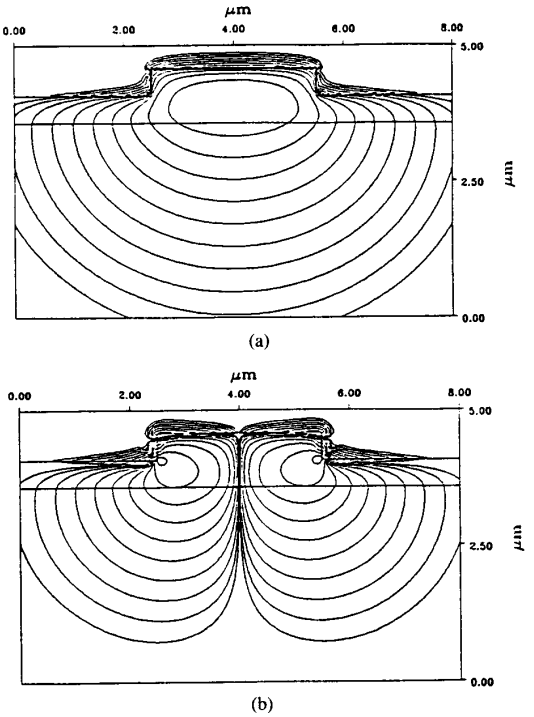

Fig. 7. The patterns of the transverse electric field for the quasi-TM mode of the rib waveguide. The waveguide parameters are $W = 3.0$ μm and $D = H = 0.5$ μm. (a) E_x; (b) E_y.

TABLE I
THE NORMALIZED PROPAGATION CONSTANTS OF THE QUASI-TE AND QUASI-TM MODES OF THE RIB WAVEGUIDE AS FUNCTIONS OF D. BPM: THIS PAPER; FD: [16]

D (μm)	Scalar		Semi-TE		Semi-TM		Full-TE BPM	Full-TM BPM
	BPM	FD	BPM	FD	BPM	FD		
0.0	0.3080	0.3071	0.3001	0.2959	0.2664	0.2617	0.3011	0.2667
0.1	0.3103	0.3094	0.3026	0.2987	0.2685	0.2639	0.3039	0.2690
0.2	0.3139	0.3129	0.3066	0.3029	0.2720	0.2672	0.3089	0.2729
0.3	0.3184	0.3179	0.3116	0.3088	0.2762	0.2718	0.3144	0.2776
0.4	0.3249	0.3245	0.3188	0.3165	0.2823	0.2780	0.3215	0.2839
0.5	0.3322	0.3330	0.3269	0.3263	0.2892	0.2862	0.3303	0.2915
0.6	0.3423	0.3436	0.3380	0.3382	0.2990	0.2964	0.3415	0.3016
0.7	0.3536	0.3563	0.3504	0.3525	0.3101	0.3089	0.3533	0.3127
0.8	0.3676	0.3719	0.3655	0.3696	0.3237	0.3245	0.3669	0.3250
0.9	0.3880	0.3914	0.3871	0.3905	0.3441	0.3448	0.3879	0.3451
1.0	0.4273	0.4319	0.4273	0.4319	0.3854	0.3863	0.4273	0.3854

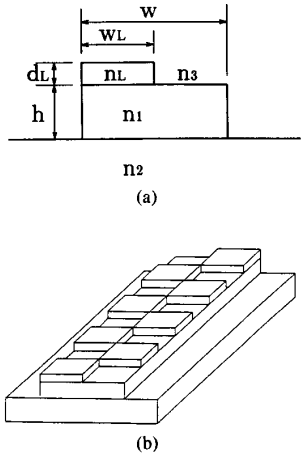

Fig. 8. A schematic diagram of the rib waveguide polarization converter. (a) The cross-sectional view and (b) the top view.

The refractive indices of waveguide are $n_1 = 3.40$, $n_2 = n_L = 3.27$, $n_3 = 1.0$. The width and the height of the guiding region are $w = 3.0$ μm and $h = 0.5$ μm. The width of dielectric loading is $w_L = 1.5$ μm and the thickness of the load is $d_L = 0.1$ μm. The wavelength is $\lambda = 1.3$ μm. Fig. 9(a) and (b) show the patterns of the dominant polarized transverse electric fields for the quasi-TE and the quasi-TM modes that are supported by the waveguide. Due to the hybrid nature of the fields, there is a minor transverse electric component with orthogonal polarization associated with each of the major components. Therefore, when a linearly polarized field is incident at the input, it will excite a combination of both the quasi-TE and the quasi-TM modes. Suppose that the dielectric loading is placed asymmetrically only on one side of the rib. The two modes will beat with each other when propagating along the waveguide and cause a slight change of the polarization. Fig. 10 shows the guided powers carried by the two polarizations as functions of propagation distance. If the dielectric loading is placed alternatively on the both sides of the rib and the period of the loading is

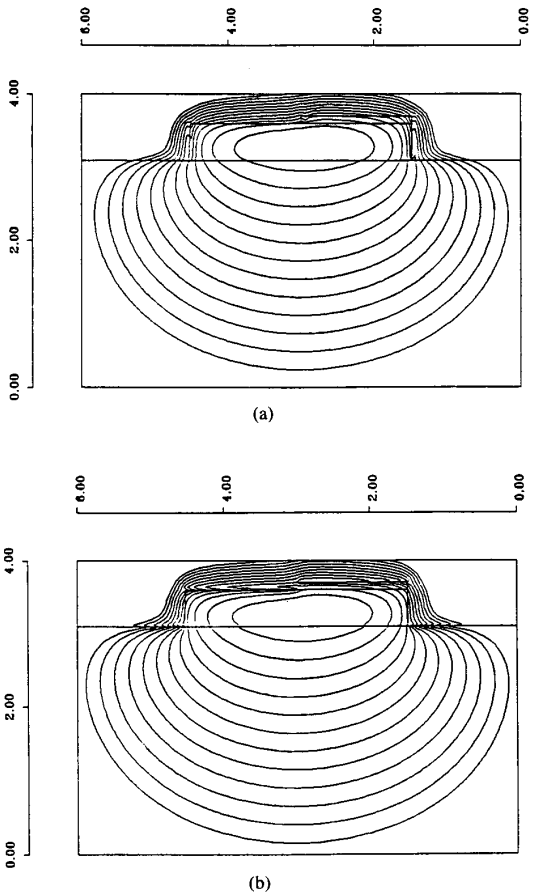

Fig. 9. The field patterns of the dominant transverse electric fields for the guided-modes supported by the asymmetrically loaded rib waveguide. (a) E_x of the quasi-TE mode; (b) E_y of the quasi-TM mode.

equal to the beat length between the two modes, then the two modes will interfere constructively and a complete polarization rotation will occur. The guided powers in the x and y polarizations as functions of propagating distance are simulated and shown in Fig. 11. Very efficient polar-

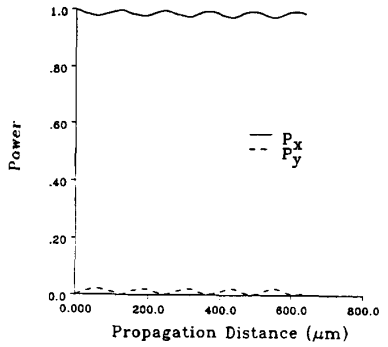

Fig. 10. The guided powers in the x and the y polarizations as functions of the propagation distance when the dielectric loading is placed only along one side of the rib. The oscillation is due to the heating between the two hybrid modes.

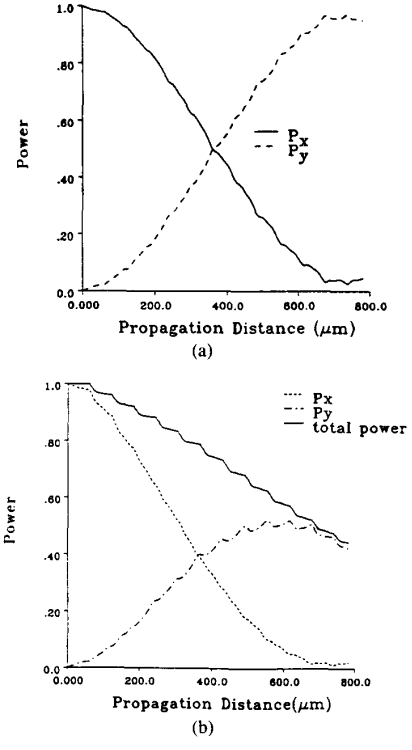

Fig. 11. The power exchange between the two polarizations as functions of the propagation distance. Solid: P_x; dot: P_y. (a) Radiation loss excluded and (b) radiation loss included.

ization coupling (a complete rotation within 800 μm) is demonstrated. Fig. 11(a) shows the guided powers excluding the radiation loss and the effect of the radiation loss is illustrated in Fig. 11(b). It is noted that the device simulated suffers about 3 dB scattering loss for one coupling length. This is mainly due to the scattering at the discontinuities along the waveguide axis.

References

[1] M. D. Feit and J. A. Fleck, Jr., "Light propagation in graded-index optical fibers," *Appl. Opt.*, vol. 17, no. 24, pp. 3990–3998, 1978.

[2] M. D. Feit and J. A. Fleck, Jr., "Computation of mode properties in optical fiber waveguides by a propagating beam method," *Appl. Opt.*, vol. 19. no. 7, pp. 1154–1163, 1980.

[3] P. Danielsen, "Two-dimensional propagating beam analysis of an electrooptic waveguide modulator," *IEEE J. Quantum Electron.*, vol. 20, pp. 1093–1097, Sept. 1984.

[4] A. Neyer, W. Mevenkamp, L. Thylen, and B. Lagerstrom, "A beam propagation method analysis of active and passive waveguide crossings," *IEEE J. Lightwave Technol.*, vol. 3, pp. 635–642, Mar. 1985.

[5] L. Thylen, E. M. Wright, G. I. Stegeman, C. T. Seaton, and J. V. Moloney, "Beam-propagation method analysis of a nonlinear directional coupler," *Opt. Lett.*, vol. 11, no. 11, pp. 739–741, 1986.

[6] D. Yevick and B. Hermansson, "New formulations of the matrix beam propagation method: Application of rib waveguides," *IEEE J. Quantum Electron.*, vol. 25, pp. 221–229, Feb. 1989.

[7] D. Yevick and B. Hermansson, "Efficient beam propagation techniques," *IEEE Quantum Electron.*, vol. 26, pp. 109–112, Jan. 1990.

[8] B. Hermansson, D. Yevick, W. Bardyszewski, and M. Glasner, "The unitary of split-operator finite difference and finite-element methods: Applications to longitudinally varying semiconductor rib waveguides," *IEEE J. Lightwave Technol.*, vol. 8, pp. 1866–1873, Dec. 1990.

[9] Y. Chung and N. Dagli, "Explicit finite difference beam propagation method: Application to semiconductor rib waveguide Y-junction analysis," *Electron. Lett.*, vol. 26, no. 11, pp. 711–713, 1990.

[10] Y. Chung and N. Dagli, "An assessment of finite difference beam propagation method," *IEEE J. Quantum Electron.*, vol. 26, pp. 1335–1339, Aug. 1990.

[11] R. Scarmozzino and R. M. Osgood, Jr., "Comparison of finite-difference and Fourier-transform solutions of the parabolic wave equation with emphasis on integrated-optics applications," *J. Opt. Soc. Amer. A*, vol. 8, no. 5, pp. 727–731, 1991.

[12] H. Kogelnik, "Theory of optical waveguides," in *Guided-Wave Optoelectronics*, T. Tamir, Ed. Berlin, Germany: Springer-Verlag, 1988.

[13] W. P. Huang and H. A. Haus, "A simple variational approach to optical rib waveguides," *IEEE J. Lightwave Technol.*, vol. 9, pp. 56–61, Jan. 1991.

[14] P. W. A. McIlroy, M. S. Stern, and P. C. Kendall, "Fast and accurate method for calculation of polarised modes in semiconductor rib waveguides," *Electron. Lett.*, vol. 25, no. 23, pp. 1586–1587, 1989.

[15] B. M. A. Rahman and J. B. Davies, "Vector-H finite element solutions of GaAs/GaAlAs rib waveguides," *IEE Proc. J.*, vol. 132, no. 6, pp. 349–353, 1985.

[16] M. Stern, "Semivectorial polarized finite difference method for optical waveguides with arbitrary index profiles," *IEE Proc. J.*, vol. 135, no. 1, pp. 56–63, 1988.

[17] D. Marcuse, *Theory of Dielectric Optical Waveguides*. New York: Academic, 1974.

[18] A. W. Snyder and J. D. Love, *Optical Waveguide Theory*. London, UK: Chapman and Hall, 1983.

[19] A. Hardy and W. Streifer, "Coupled-mode theory of parallel waveguides," *IEEE J. Lightwave Technol.*, vol. 3, pp. 1135–1146, 1985.

[20] H. A. Haus, W. P. Huang, S. Kawakami, and N. A. Whitaker, "Coupled mode theory of optical waveguides," *IEEE J. Lightwave Technol.*, vol. 5, pp. 16–23, Jan. 1987.

[21] S. L. Chuang, "A coupled mode formulation by reciprocity and a variational principle," *IEEE J. Lightwave Technol.*, vol. 5, pp. 5–15, Jan. 1987.

[22] W. P. Huang, S. T. Chu, and S. K. Chaudhuri, "A scalar coupled-mode theory with vector correction," *IEEE J. Quantum Electron.*, vol. 28, pp. 184–193, Jan. 1992.

[23] W. P. Huang, C. L. Xu, and S. K. Chaudhuri, "Modeling and analysis of fiber-optic mode transducer. Single fiber with periodic perturbation," *IEEE J. Lightwave Technol.*, vol. 9, pp. 1431–1438, Nov. 1991.

[24] W. P. Huang and Z. M. Mao, "Polarization rotation in periodically loaded rib waveguides," *IEEE J. Lightwave Technol.*, vol. 11, Oct. 1993.

[25] T. B. Koch, J. B. Davies, and D. Wickramasinghe, "Finite element/Finite difference propagation algorithm for integrated optical device," *Electron. Lett.*, vol. 25, no. 8, pp. 514–516, 1989.

[26] R. Clauberg and P. Von Allmen, "Vectorial beam-propagation method for integrated optics," *Electron. Lett.*, vol. 27, no. 8, pp. 654–655, 1991.

[27] W. P. Huang, C. L. Xu, S. T. Chu, and S. K. Chaudhuri, "A vector

beam propagation method for guided-wave optics," *IEEE Photon. Tech. Lett.*, vol. 3, pp. 910–913, Oct. 1991.
[28] W. P. Huang, C. L. Xu, and S. K. Chaudhuri, "A finite-difference vector beam propagation method for three-dimensional structures," *IEEE Photon. Tech. Lett.*, vol. 4, pp. 148–151, Feb. 1992.
[29] W. P. Huang, C. L. Xu, and S. K. Chaudhuri, "A finite-difference vector beam propagation method based on H-fields," *IEEE Photon. Tech. Lett.*, vol. 3, pp. 1117–1120, Dec. 1991.
[30] W. P. Huang, C. L. Xu, S. T. Chu, and S. K. Chaudhuri, "The finite-difference vector beam propagation method. Analysis and Assessment," *IEEE J. Lightwave Technol.*, vol. 10, pp. 295–305, Mar. 1992.
[31] W. P. Huang, C. L. Xu, and S. K. Chaudhuri, "Application of the finite difference vector beam propagation method to directional coupler devices," *IEEE J. Quantum Electron.*, vol. 28, pp. 1527–1532, June 1992.
[32] A. Behie and P. K. W. Vinsome, "Block iterative methods for fully implicit reservoir simulation," *Soc. Pet. Eng. J.*, pp. 658–668, Oct. 1982.
[33] G. Ronald Hadley, "Transparent boundary condition for the beam propagation method," *IEEE Quantum Electron.*, vol. 28, pp. 363–370, Jan. 1990.
[34] D. Yevick and M. Glasner, "Fresnel and wide-angle equation analyses of microlenses," *IEEE Photon. Technol. Lett.*, vol. 2, pp. 413–414, June 1990.
[35] C. L. Xu, W. P. Huang, and S. K. Chaudhuri, "Efficient and accurate vector mode calculations by beam propagation method," *IEEE J. Lightwave Technol.*, vol. 11, Oct. 1993.
[36] Y. Shani, R. Alferness, T. Koch, U. Koren, M. Oron, B. I. Miller, and M. G. Young, "Polarization rotation in asymmetric periodic loaded rib waveguides," *Appl. Phys. Lett.*, vol. 59, no. 11, pp. 1278–1280, 1991.

H. P. Huang (M'89), for a photograph and biography, see p. 183 of the January 1992 issue of this JOURNAL.

C. L. Xu, for a photograph and biography, see p. 1532 of the June 1992 issue of this JOURNAL.